TECHNISCHE MECHANIK
an open access journal

journal homepage: www.ovgu.de/techmech

Tech. Mech., Vol. 40, Is. 2, (2020), 120–133

Received: 18.02.2020
Accepted: 25.03.2020
Available online: 06.04.2020

On the Analytical Estimation for Isotropic Approximation of Elastic Properties applied to Polycrystalline Cubic Silicon used at Solar Cells

Marcus Aßmus*, Rainer Glüge, Holm Altenbach

Otto von Guericke University, Institute of Mechanics, Universitätsplatz 2, 39108 Magdeburg, Germany

Abstract: The present contribution is concerned with the effective mechanical parameters of polycristalline silicon used for solar cells. Thereby, an analytical scheme for the prediction of elastic properties of polycrystals is reviewed, applied and verified. Emphasis is on first-order bounds and derived estimates. Based on cubic symmetry of a single crystal the projector representation is exploited for the description of the constitutive equations. The elasticity tensor is developed for several assumptions which stem from rather classical homogenization schemes. This results in a rational representation and determination of linear elastic material parameters of a homogeneous, macroscopically isotropic comparison material. The analytically determined parameters are compared to experimental data. It is found that the present procedure reproduces the experimental results in very close proximity.

Keywords: solar energy materials, solar cells, polycrystals, cubic system, homogenization, mechanical properties

1 Introduction

Silicon is the most commonly used semiconductor material for solar cells in photovoltaic modules. The actual market share is around 90% (Philipps and Warmuth, 2019). Basically a distinction is here made between mono- and polycrystalline silicon. Although higher electrical efficiencies can be achieved with monocrystalline silicon, polycrystalline silicon is used more widely with a market share of approximately 65%. This is not least due to its cheaper production (Philipps and Warmuth, 2019) whereby in principle several fabrication methods are possible (Petersen, 1982). During the service life of photovoltaic modules, the built-in solar cells are exposed to different mechanical loading scenarios. To name two extremes as an example, high snow loads at low temperatures far below freezing point or high wind loads at temperatures above 60 degrees Celsius can occur. The specification of the temperature is important here since the solar cells are embedded in an encapsulant whose material is strongly temperature sensitive. Solar cells should be able to withstand these stresses for periods of at least 20 years. From an engineering point of view, strength analyses are necessary therefore. Such analyses are of immense importance since failures at solar cells are correlated with power loss and decreased energy harvest (Köntges et al., 2014).
In present work we will focus on polycrystalline silicon. Aggregates of silicon consist of monocrystals obeying a cubic symmetry. Due to the complexity of geometrical models for such aggregates, the necessity often arises to work with a comparison medium for the discrete microstructure. It is in particular advantageous to work with effective properties during the design process for structural analysis. According to Petersen (1982), the effective Young's modulus of polycrystalline silicon is around $150 \cdot 10^3$ to $170 \cdot 10^3$ $\mathrm{N/mm^2}$, referring to various sources. This is certainly a very broad range ($\Delta_Y = 20 \cdot 10^3$ $\mathrm{N/mm^2}$), which means that results of strength analysis will spread over an equally broad area. This is why there are various efforts to substantiate effective values of polycrystalline silicon, cf. (Hopcraft et al., 2010).
In mechanics, computational and analytical methods for such estimations have proven successful, cf. Böhm (2020). The attraction of an analytical method lies in its usually simple handling and the rapid attainment of results, at least in comparison to computational methods. In the context of analytical homogenization methods, first-order (Voigt, 1889; Reuss, 1929) and second-order (Hashin and Shtrikman, 1962a,b) estimates, self-consistant estimates (Christensen and Lo, 1979) and statistical methods (Kröner, 1958) exist. Basic reviews of different methods to determine effective elastic parameters are presented in Kröner (1972) or Lobos Fernãndez (2018). If the morphology of the microstructure is sufficiently isotropic first-order estimates deliver results with sufficient accuracy. The following assumptions are made in the course of present investigations.

- We consider silicon mono- and polycrystals where physical and geometrical linearity is a reasonable assumption in the elastic range.
- The silicon monocrystal possesses a cubic crystal symmetry.
- The crystal orientation of the bulk features a uniform distribution.
- The interaction of the crystals and the influence of the distribution functions of the crystal interfaces and the crystal edges on the symmetry of the macroscopic elastic behavior are neglected.

The consideration of a uniform distribution of the crystal orientation is equivalent to an isotropic crystal orientation function. Morphological investigations of solar cells showed crystallographic textures with no evidence of preferred orientation Stokkan et al. (2018), at least in the preferential range of moderate cooling rates during production, cf. Yang et al. (2015). The

* E-mail address: marcus.assmus@ovgu.de
doi: 10.24352/UB.OVGU-2020-020

above mentioned assumption does therefore not contradict physical reality. In context of a preferably accurate prediction for a polycrystal consisting of cubic monocrystals, a discrete number of crystals is necessary to guarantee statistically isotropy of the bulk. Following Elvin (1996) this is around 230 crystals while rds (2003) provides a specific equation obeying the convergence of the prediction error via the increase of the number of crystals. Compared with Basore (1994), this restriction seems sufficiently fulfilled with polycrystalline silicon solar cells. Nevertheless, these values do not seem to bound the possible crystal numbers. It is important to note that the present analytical approaches are based on an infinite number of crystals (Hill, 1952). The resulting approximations therefore loose quality with decreasing crystal numbers. However, since the contrast of the elastic properties of the components made of polycrystalline silicon is comparatively small, the first-order estimates incorporating the restrictions named above result in comparatively close approximations.

Notation. Throughout the whole text, a direct tensor notation is preferred. First- and second-order tensors are denoted by lowercase and uppercase bold letters, e.g., $\boldsymbol{a}$ and $\boldsymbol{A}$, respectively. Fourth-order tensors are designated by uppercase blackboard bold letters, e.g. $\mathbb{A}$. In continuation, some operations between these tensors need to be defined which will be done based on a three-dimensional orthonormal basis. For indices $i, j, k, \ldots \in \{1, 2, 3\}$ holds. The Einstein summation convention is applied. Common operations are the dyadic product

$$\boldsymbol{a} \otimes \boldsymbol{b} = a_i b_j \boldsymbol{e}_i \otimes \boldsymbol{e}_j = \boldsymbol{C}\,, \tag{1}$$

the scalar product

$$\boldsymbol{a} \cdot \boldsymbol{b} = a_i b_j \boldsymbol{e}_i \cdot \boldsymbol{e}_j = a_i b_i = c\,, \tag{2}$$

the composition of a second- and a first-order tensor

$$\boldsymbol{A} \cdot \boldsymbol{a} = A_{lm} a_i \boldsymbol{e}_l \otimes \boldsymbol{e}_m \cdot \boldsymbol{e}_i = A_{li} a_i \boldsymbol{e}_l = \boldsymbol{d}\,, \tag{3}$$

the composition of two second-order tensors

$$\boldsymbol{A} \cdot \boldsymbol{B} = A_{lm} B_{no} \boldsymbol{e}_l \otimes \boldsymbol{e}_m \cdot \boldsymbol{e}_n \otimes \boldsymbol{e}_o = A_{lm} B_{mo} \boldsymbol{e}_l \otimes \boldsymbol{e}_o = \boldsymbol{D}\,, \tag{4}$$

the double scalar product between two second-order tensors

$$\boldsymbol{A} : \boldsymbol{B} = A_{lm} B_{no} \boldsymbol{e}_l \otimes \boldsymbol{e}_m : \boldsymbol{e}_n \otimes \boldsymbol{e}_o = A_{lm} B_{lm} = d\,, \tag{5}$$

the double scalar product between a fourth- and a second-order tensor

$$\mathbb{A} : \boldsymbol{B} = A_{pqrs} B_{no} \boldsymbol{e}_p \otimes \boldsymbol{e}_q \otimes \boldsymbol{e}_r \otimes \boldsymbol{e}_s : \boldsymbol{e}_n \otimes \boldsymbol{e}_o = A_{pqrs} B_{rs} \boldsymbol{e}_p \otimes \boldsymbol{e}_q = \boldsymbol{E}\,, \tag{6}$$

the double scalar product between two fourth-order tensors

$$\mathbb{A} : \mathbb{B} = A_{pqrs} B_{tuvw} \boldsymbol{e}_p \otimes \boldsymbol{e}_q \otimes \boldsymbol{e}_r \otimes \boldsymbol{e}_s : \boldsymbol{e}_t \otimes \boldsymbol{e}_u \otimes \boldsymbol{e}_v \otimes \boldsymbol{e}_w = A_{pqrs} B_{rsvw} \boldsymbol{e}_p \otimes \boldsymbol{e}_q \otimes \boldsymbol{e}_v \otimes \boldsymbol{e}_w = \mathbb{F}\,, \tag{7}$$

and the fourfold scalar product between two fourth-order tensors

$$\mathbb{A} :: \mathbb{B} = A_{pqrs} B_{tuvw} \boldsymbol{e}_p \otimes \boldsymbol{e}_q \otimes \boldsymbol{e}_r \otimes \boldsymbol{e}_s :: \boldsymbol{e}_t \otimes \boldsymbol{e}_u \otimes \boldsymbol{e}_v \otimes \boldsymbol{e}_w = A_{pqrs} B_{pqrs} = g\,. \tag{8}$$

The inverse of a tensor is defined by

$$\boldsymbol{A}^{-1} \cdot \boldsymbol{A} = \boldsymbol{A} \cdot \boldsymbol{A}^{-1} = \boldsymbol{1} \tag{9}$$

while the transposed of a tensor is given by

$$\boldsymbol{a} \cdot \boldsymbol{A}^{\top} \cdot \boldsymbol{b} = \boldsymbol{b} \cdot \boldsymbol{A} \cdot \boldsymbol{a}\,. \tag{10}$$

Herein, $\boldsymbol{1} = \boldsymbol{e}_i \otimes \boldsymbol{e}_i$ is the identity on first order tensors. For an orthogonal tensor, $\boldsymbol{B}^{-1} = \boldsymbol{B}^{\top}$ holds true. We furthermore introduce the Rayleigh product which maps all basis vectors of a tensor simultaneously without changing components. It is defined for a dyad and a tensor of arbitrary order. E.g., when applied to a tetrad, the product is

$$\boldsymbol{B} \star \mathbb{A} = A_{ijkl} (\boldsymbol{B} \cdot \boldsymbol{e}_i) \otimes (\boldsymbol{B} \cdot \boldsymbol{e}_j) \otimes (\boldsymbol{B} \cdot \boldsymbol{e}_k) \otimes (\boldsymbol{B} \cdot \boldsymbol{e}_l) \qquad \text{with } A_{ijkl} = \mathbb{A} :: \boldsymbol{e}_i \otimes \boldsymbol{e}_j \otimes \boldsymbol{e}_k \otimes \boldsymbol{e}_l. \tag{11}$$

The Frobenius norm of fourth-, second, and first-order tensors is defined as follows.

$$\|\mathbb{A}\| = [\mathbb{A} :: \mathbb{A}]^{\frac{1}{2}} \qquad \|\boldsymbol{A}\| = [\boldsymbol{A} : \boldsymbol{A}]^{\frac{1}{2}} \qquad \|\boldsymbol{a}\| = [\boldsymbol{a} \cdot \boldsymbol{a}]^{\frac{1}{2}} \tag{12}$$

Overlined quantities indicate effective measures.

2 Theoretical Background

Silicon is a brittle material. Its mechanical behaviour is characterised by linear elasticity until fracture. This legitimates the use of Hooke's law. Considering a polycrystalline aggregate, the linear relation between stress $\boldsymbol{T}$ and strain $\boldsymbol{E}$ holds true for every single crystal.

$$\boldsymbol{T} = \mathbb{C} \colon \boldsymbol{E} \tag{13}$$

Using the eigenprojector representation, it is possible to represent the stiffness tensor $\mathbb{C}$ as a linear combination of eigenprojectors $\mathbb{P}_J$ and eigenvalues λ_J (Halmos, 1958; Mehrabadi and Cowin, 1990).

$$\mathbb{C} = \sum_{J=1}^{Z} \lambda_J \mathbb{P}_J \tag{14}$$

In general, the number of distinct eigenvalues λ_J of $\mathbb{C}$ is in the range $2 \leq Z \leq 6$. Any admissible set of projectors fulfil subsequent projector rules (Rychlewski, 1995).

$$\mathbb{P}_J \colon \mathbb{P}_J = \mathbb{P}_J \qquad \mathbb{P}_J \colon \mathbb{P}_L = \mathbb{O} \quad \forall\, J \neq L \qquad \sum \mathbb{P}_J = \mathbb{I}^{\mathrm{sym}} \qquad \mathbb{P}_J :: \mathbb{P}_J = NS \tag{15}$$

Herein, NS is the number of dimensions of the subspace. In the case of cubic symmetry (superscript c), this method results in $Z = 3$ distinct eigenvalues and projectors.

$$\mathbb{C}^{\mathrm{c}} = \lambda_1^{\mathrm{c}} \mathbb{P}_1^{\mathrm{c}} + \lambda_2^{\mathrm{c}} \mathbb{P}_2^{\mathrm{c}} + \lambda_3^{\mathrm{c}} \mathbb{P}_3^{\mathrm{c}} \tag{16}$$

The projectors are expressed as follows (Rychlewski and Zhang, 1989).

$$\mathbb{P}_1^{\mathrm{c}} = \frac{1}{3} \boldsymbol{1} \otimes \boldsymbol{1} \qquad \mathbb{P}_2^{\mathrm{c}} = \mathbb{D} - \mathbb{P}_1^{\mathrm{c}} \qquad \mathbb{P}_3^{\mathrm{c}} = \mathbb{I}^{\mathrm{sym}} - \left(\mathbb{P}_1^{\mathrm{c}} + \mathbb{P}_2^{\mathrm{c}} \right) \tag{17}$$

The second and the third cubic projectors contain the anisotropic portion

$$\mathbb{D} = \sum_{i=1}^{3} \boldsymbol{g}_i \otimes \boldsymbol{g}_i \otimes \boldsymbol{g}_i \otimes \boldsymbol{g}_i = \boldsymbol{Q} \star \sum_{i=1}^{3} \boldsymbol{e}_i \otimes \boldsymbol{e}_i \otimes \boldsymbol{e}_i \otimes \boldsymbol{e}_i \tag{18}$$

where $\boldsymbol{g}_i \;\forall\, i = \{1, 2, 3\}$ denote the orthonormal lattice vectors of the single crystal, which are related to a fixed (sample) reference basis $\boldsymbol{e}_i \;\forall\, i = \{1, 2, 3\}$ by means of an proper orthogonal tensors $\boldsymbol{Q}$, e.g. $\boldsymbol{g}_i = \boldsymbol{Q} \cdot \boldsymbol{e}_i$. Furthermore, $2\mathbb{I}^{\mathrm{sym}} = \boldsymbol{e}_i \otimes \boldsymbol{e}_j \otimes \left(\boldsymbol{e}_i \otimes \boldsymbol{e}_j + \boldsymbol{e}_j \otimes \boldsymbol{e}_i \right)$ is the identity on symmetric second-order tensors. The eigenvalues are determined by the projection of the constitutive tensor onto the space of the respective symmetry group.

$$\lambda_J = \mathbb{C} :: \frac{\mathbb{P}_J}{\| \mathbb{P}_J \|^2} \tag{19}$$

The three distinct eigenvalues in Eq. (16) are as follows with respect to the lattice vectors $\boldsymbol{g}_i$ (Sutcliffe, 1992).

$$\lambda_1^{\mathrm{c}} = C_{1111} + 2C_{1122}, \qquad \lambda_2^{\mathrm{c}} = C_{1111} - C_{1122}, \qquad \lambda_3^{\mathrm{c}} = 2C_{2323} \tag{20}$$

The degree of anisotropy of the cubic single crystals can be described as $\lambda_3^{\mathrm{c}} - \lambda_2^{\mathrm{c}}$, turning to zero in the case of isotropy. By the aid of the projector representation, it is trivial to determine the inverse of the stiffness tensor.

$$\left(\mathbb{C}^{\mathrm{c}} \right)^{-1} = \frac{1}{\lambda_1^{\mathrm{c}}} \mathbb{P}_1^{\mathrm{c}} + \frac{1}{\lambda_2^{\mathrm{c}}} \mathbb{P}_2^{\mathrm{c}} + \frac{1}{\lambda_3^{\mathrm{c}}} \mathbb{P}_3^{\mathrm{c}} = \mathbb{S}^{\mathrm{c}} \tag{21}$$

In analogy to Eq. (19), the eigenvalues are determined by taking the sclar product of the projectors and this compliance.

$$\frac{1}{\lambda_J} = \mathbb{S} :: \frac{\mathbb{P}_J}{\| \mathbb{P}_J \|^2} \tag{22}$$

First endeavors to determine the overall elasticity tensor of polycrystals were made by Woldemar Voigt and AndrÃąs (Endre) Reuss. Voigt (1889) assumed a uniform, i.e., isotropic crystal orientation distribution function and a homogeneous strain field in the aggregate. Reuss (1929) suggested an corresponing estimate based on a homogeneous orientation distribution function and a homogeneous stress field. Generally, these volume averages are anisotropic. If and only if the polycrystal contains a sufficiently large number of crystals, macroscopic homogeneity and isotropy results (Hill, 1952), i.e. the texture is vanishing. For such isotropic microstructures, the crystals differ only with respect to their orientation. The approaches by Voigt and Reuss can be written as follows.

$$\mathbb{C}^{\mathrm{V}} = \int_Q f(\boldsymbol{Q})\, \mathbb{C}^{\mathrm{c}}(\boldsymbol{Q})\, \mathrm{d}Q \qquad \mathbb{S}^{\mathrm{R}} = \int_Q f(\boldsymbol{Q})\, \mathbb{S}^{\mathrm{c}}(\boldsymbol{Q})\, \mathrm{d}Q \tag{23}$$

Herein $f(\boldsymbol{Q})$ specifies the volume fraction ${}^{\mathrm{d}V}/_{V}$ of crystals with the orientation $\boldsymbol{Q}$ (Bunge, 1965) and dQ is the volume element in $\mathcal{SO}_3$ (special orthogonal group). Obviously, $\mathbb{C}^{\mathrm{R}} \neq \mathbb{C}^{\mathrm{V}}$ holds. These arithmetic and harmonic means of the stiffness tensors correspond to the assumption of homogeneous strain and stress fields, respectively. If only discrete orientations are of interest as in the case of polycrystalline silicon, the average over the orientation space can be formulated as weighted sum of the crystals volume fraction corresponding to the specific orientation and the affiliated elasticity tensor.

$$\mathbb{C}^{\mathrm{V}} = \sum_{\gamma=1}^{\eta} v_\gamma \mathbb{C}^{\mathrm{c}}_\gamma \qquad\qquad \mathbb{S}^{\mathrm{R}} = \sum_{\gamma=1}^{\eta} v_\gamma \mathbb{S}^{\mathrm{c}}_\gamma \tag{24}$$

Herein, η represents the number of crystals under consideration. Both estimates result in macroscopically isotropic elasticity parameters. In context of the elasticity tensor $\mathbb{C}^{\mathrm{c}}$, the coincidence of the second and third eigenvalue is a necessary and sufficient condition for an isotropic material. Hence, expression (16) reduces as follows whereby $Z = 2$ holds true in view of Eq. (14).

$$\mathbb{C}^{\circ} = \lambda_1^{\circ}\mathbb{P}_1^{\circ} + \lambda_2^{\circ}\mathbb{P}_2^{\circ} \tag{25}$$

We can furthermore introduce the isotropic compliance.

$$\left(\mathbb{C}^{\circ}\right)^{-1} = \frac{1}{\lambda_1^{\circ}}\mathbb{P}_1^{\circ} + \frac{1}{\lambda_2^{\circ}}\mathbb{P}_2^{\circ} = \mathbb{S}^{\circ} \tag{26}$$

While the first projector coincides with the one of the cubic case ($\mathbb{P}_1^{\circ} = \mathbb{P}_1^{\mathrm{c}}$), the second is determined as follows.

$$\mathbb{P}_2^{\circ} = \mathbb{P}_2^{\mathrm{c}} + \mathbb{P}_3^{\mathrm{c}} = \mathbb{I}^{\mathrm{sym}} - \mathbb{P}_1^{\circ} \tag{27}$$

Due to the isotropic nature of volumetric changes in case of cubic crystal symmetry, $\lambda_1^{\circ} = \lambda_1^{\mathrm{c}}$ holds true (Hill, 1952). In the isotropic case, $\lambda_2^{\circ} = C_{1111} - C_{1122} = 2C_{2323}$ also holds. Considering the second eigenvalue for an isotropic comparison material arising from the average theorems mentioned above, the second and third eigenvalue of the cubic symmetry have to be weighted according to their deviator space dimensions, cf. Walpole (1984) and Rychlewski (1984). This requires an allocation for λ_2°, either to the Voigt (homogeneous strain) or the Reuss (homogeneous stress) assumption ($\lambda_2^{\mathrm{V}} \veebar \lambda_2^{\mathrm{R}}$).

$$\lambda_2^{\mathrm{V}} = \frac{2}{5}\lambda_2^{\mathrm{c}} + \frac{3}{5}\lambda_3^{\mathrm{c}} \qquad\qquad \lambda_2^{\mathrm{R}} = \left[\frac{2}{5}\frac{1}{\lambda_2^{\mathrm{c}}} + \frac{3}{5}\frac{1}{\lambda_3^{\mathrm{c}}}\right]^{-1} \tag{28}$$

Above introduced stiffnesses constitute upper and lower bounds of the strain energy density (Nemat-Nasser and Hori, 1993). To be exact, the Voigt bound is equal to the first-order upper bound, whereas the Reuss bound equals the first-order lower bound. It was found by Hill (1952) that the range for the true effective stiffness $\overline{\mathbb{C}}$ is bounded by the Voigt (arithmetic) and the Reuss (harmonic) estimate. In the sense of positive definiteness ($\boldsymbol{A}\boldsymbol{:}\mathbb{C}\boldsymbol{:}\boldsymbol{A} > 0 \;\forall\, \boldsymbol{A} \neq \boldsymbol{0}$) we can state the following.

$$\mathbb{C}^{\mathrm{V}} \geq \overline{\mathbb{C}} \geq \mathbb{C}^{\mathrm{R}} \tag{29}$$

Hill (1952) suggested an arithmetic (H+) and an geometric mean (H-) of these isotropic bounds as good approximations, whereby these statements are based on pure empiricism.

$$\mathbb{C}^{\mathrm{H}+} = \frac{1}{2}\left[\mathbb{C}^{\mathrm{V}} + \mathbb{C}^{\mathrm{R}}\right] \qquad\qquad \mathbb{C}^{\mathrm{H}-} = \exp\left(\frac{1}{2}\left[\log\mathbb{C}^{\mathrm{V}} + \log\mathbb{C}^{\mathrm{R}}\right]\right) \tag{30}$$

The latter is usually ignored in the literature, c.f. Morawiec (2004). Herein, we can introduce $\log\mathbb{C} = \sum \log(\lambda_J)\,\mathbb{P}_J$ and $\exp\mathbb{C} = \sum \exp(\lambda_J)\,\mathbb{P}_J$ since $J \in \{1, 2\}$ holds. Using such representation and considering the projector rules introduced in Eqs. (15), Eqs. (30) can be easily transformed into the subsequent form.

$$\mathbb{C}^{\mathrm{H}+} = \lambda_1^{\mathrm{H}+}\mathbb{P}_1^{\circ} + \lambda_2^{\mathrm{H}+}\mathbb{P}_2^{\circ} \qquad\qquad \mathbb{C}^{\mathrm{H}-} = \lambda_1^{\mathrm{H}-}\mathbb{P}_1^{\circ} + \lambda_2^{\mathrm{H}-}\mathbb{P}_2^{\circ} \tag{31}$$

Herein, $\lambda_1^{\mathrm{H}-} = \lambda_1^{\mathrm{H}+} = \lambda_1^{\circ} = \lambda_1^{\mathrm{c}}$ hold true since $\lambda_1^{\mathrm{V}} = \lambda_1^{\mathrm{R}}$ is valid. For the second eigenvalues $\lambda_2^{\mathrm{H}\pm}\;\forall \pm \in \{+ \vee -\}$, the arithmetic and the geometric mean holds, respectively.

$$\lambda_2^{\mathrm{H}+} = \frac{1}{2}\left[\lambda_2^{\mathrm{V}} + \lambda_2^{\mathrm{R}}\right] \qquad\qquad \lambda_2^{\mathrm{H}-} = \left[\lambda_2^{\mathrm{V}}\lambda_2^{\mathrm{R}}\right]^{\frac{1}{2}} \tag{32}$$

Since the geometric mean is smaller than the arithmetic, but both values lie inbetween the bounds of Voigt and Reuss, following representation holds.

$$\mathbb{C}_{\max} \geq \mathbb{C}^{\mathrm{V}} \geq \mathbb{C}^{\mathrm{H}+} \geq \mathbb{C}^{\mathrm{H}-} \geq \mathbb{C}^{\mathrm{R}} \geq \mathbb{C}_{\min} \tag{33}$$

However, in the literature it is often referred that the choice of the arithmetic mean is reasonable, due to a better agreement with experiments. We will deal with this proposition in a subsequent section. The orientational dependencies of the Young's modulus for a stiffness tensor $\mathbb{C}$ with arbitrary material symmetry can be presented considering the tensile direction $\boldsymbol{d}$, where $\boldsymbol{d}$ is

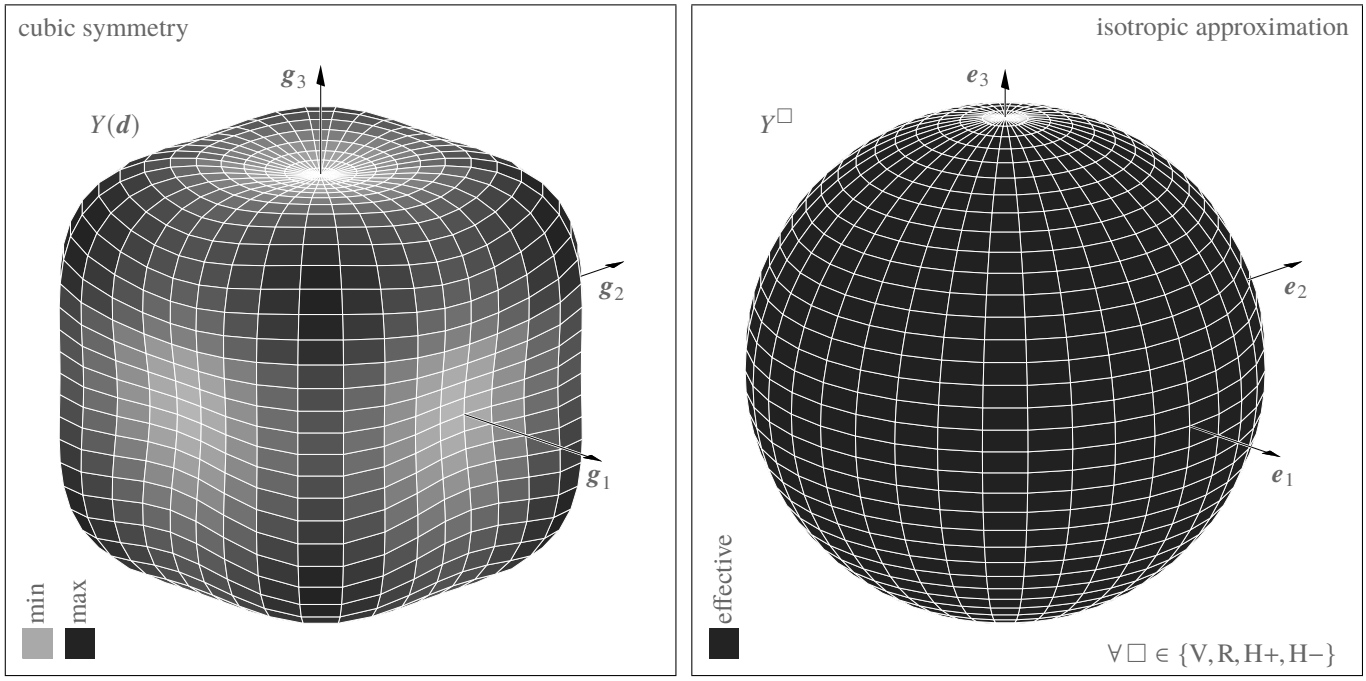

Fig. 1: Spatial plot of Young's modulus $Y(\boldsymbol{d})$ of a single crystal and isotropic approximation $Y^{\square}$ of the polycrystalline aggregate

parametrized in spherical coordinates with $\|\boldsymbol{d}\| = 1$ (Hayes, 1972; Rychlewski, 1995). Since from an experimental standpoint, the Young's modulus, defined as the ratio of stress and strain in $\boldsymbol{d}$, is measured in most cases, we confine further spatial comparisons of the different estimates to this measure.

$$Y(\boldsymbol{d}) = \left[(\boldsymbol{d} \otimes \boldsymbol{d}) : \mathbb{S}^{\square} : (\boldsymbol{d} \otimes \boldsymbol{d})\right]^{-1} \qquad \forall \square \in \{\mathrm{V}, \mathrm{R}, \mathrm{H}+, \mathrm{H}-\} \tag{34}$$

However, results of estimations based on Eq. (25) with eigenvalues (28) or (32) are isotropic approximations. Hence, it is possible to determine its orientation-independent engineering parameters.

$$Y^{\square} = \frac{3\lambda_1^{\mathrm{c}}\lambda_2^{\square}}{2\lambda_1^{\mathrm{c}} + \lambda_2^{\square}} \qquad \nu^{\square} = \frac{\lambda_1^{\mathrm{c}} - \lambda_2^{\square}}{2\lambda_1^{\mathrm{c}} + \lambda_2^{\square}} \qquad \forall \square \in \{\mathrm{V}, \mathrm{R}, \mathrm{H}+, \mathrm{H}-\} \tag{35}$$

Herein, Y is Young's modulus and ν is Poisson's ratio. Furthermore, the bulk K and the shear G moduli arise naturally.

$$3K = \lambda_1^{\mathrm{c}} \qquad 2G^{\square} = \lambda_2^{\square} \qquad \forall \square \in \{\mathrm{V}, \mathrm{R}, \mathrm{H}+, \mathrm{H}-\} \tag{36}$$

Subsequent relations emerge.

$$Y^{\square} = \frac{9KG^{\square}}{3K + G^{\square}} \qquad \nu^{\square} = \frac{3K - 2G^{\square}}{2(3K + G^{\square})} \qquad \forall \square \in \{\mathrm{V}, \mathrm{R}, \mathrm{H}+, \mathrm{H}-\} \tag{37}$$

The procedure often quoted as Voigt-Reuss-Hill average merely results in engineering parameters of the arithmetic mean $(Y^{\square}, \nu^{\square}, K^{\square}, G^{\square} \ \forall \square \in \{H+\})$.
Note that the whole procedure presented here is based on the second and third eigenvalue of the cubic system solely. As a result, the approximation of the isotropic elasticity and compliance tensor simplifies to the following expression.

$$\mathbb{C}^{\circ} = \lambda_1 \mathbb{P}_1 + \lambda_2^{\square} \mathbb{P}_2^{\circ} \qquad \forall \square \in \{\mathrm{V}, \mathrm{R}, \mathrm{H}+, \mathrm{H}-\} \tag{38}$$

Within the eigenspaces, all calculations can be traced back to scalars. This method is therewith easy to handle compared to laborious operations by application of the vector-matrix-notation, as often referred to in the literature. This simplicity and elegance is based on the projector representation.

3 Application and Results

When evaluating the results of the estimations described in the previous section, values for the cubic parameters of a single crystal are considered, which originate from Hosford (1993).

$$C_{1111} = 166.2 \cdot 10^3 \frac{\mathrm{N}}{\mathrm{mm}^2} \qquad C_{1122} = 64.4 \cdot 10^3 \frac{\mathrm{N}}{\mathrm{mm}^2} \qquad C_{2323} = 79.7 \cdot 10^3 \frac{\mathrm{N}}{\mathrm{mm}^2} \tag{39}$$

This results in subsequent eigenvalues.

$$\lambda_1^{\mathrm{c}} = 295 \cdot 10^3 \frac{\mathrm{N}}{\mathrm{mm}^2} \qquad \lambda_2^{\mathrm{c}} = 101.8 \cdot 10^3 \frac{\mathrm{N}}{\mathrm{mm}^2} \qquad \lambda_3^{\mathrm{c}} = 159.4 \cdot 10^3 \frac{\mathrm{N}}{\mathrm{mm}^2} \tag{40}$$

Tab. 1: Young's modulus Y and Poisson's ratio ν of different estimates, bounds and their spans

$Y_{\min}$	$Y_{\max}$	Y^{V}	Y^{R}	$Y^{\mathrm{H+}}$	$Y^{\mathrm{H-}}$	$\Delta_Y^{\min\max}$	Δ_Y^{VR}	$\Delta_Y^{\mathrm{H\pm}}$
$130.200{\cdot}10^3$	$188.260{\cdot}10^3$	$166.141{\cdot}10^3$	$159.773{\cdot}10^3$	$162.971{\cdot}10^3$	$162.933{\cdot}10^3$	$58.060{\cdot}10^3$	$6.368{\cdot}10^3$	38.133
$\nu_{\min}$	$\nu_{\max}$	ν^{V}	ν^{R}	$\nu^{\mathrm{H+}}$	$\nu^{\mathrm{H-}}$	$\Delta_\nu^{\min\max}$	Δ_ν^{VR}	$\Delta_\nu^{\mathrm{H\pm}}$
0.062	0.363	0.218	0.229	0.223	0.223	0.300	0.011	$6.5 \cdot 10^{-5}$

(Y in $\mathrm{N/mm^2}$, ν is dimensionless)

A common measure to quantify the extent of anisotropy in a cubic system is the Zener ratio $ZR = \lambda_3^{\mathrm{c}}/\lambda_2^{\mathrm{c}}$ (Zener, 1948). If materials are isotropic, $ZR = 1$ holds true. For material parameters of monocrystalline silicon listed in Eq. (40), $ZR \approx 1.57$ results. Compared to other cubic materials (e.g. copper, silver, gold, lead), the degree of anisotropy for monocrystalline silicon is moderate. For further anisotropy measures and physical explanations, cf. Ranganathan and Ostoja-Starzewski (2008).
For the further examinations we mainly refer to Young's modulus as it is more significant in comparison to Poisson's ratio and also has the broadest application in materials technology. The directional dependence of a single silicon crystal according to Eq. (34) shows the following parameters where seven directions are under consideration. Due to the crystallographic equivalence of some directions, only three of them are characteristic.

$$Y(\boldsymbol{d}) = \begin{cases} 130.2 \cdot 10^3 \,\frac{\mathrm{N}}{\mathrm{mm}^2} & \text{if } \boldsymbol{d} = \boldsymbol{g}_i \\ 169.4 \cdot 10^3 \,\frac{\mathrm{N}}{\mathrm{mm}^2} & \text{if } \boldsymbol{d} = \boldsymbol{n}_i \\ 188.2 \cdot 10^3 \,\frac{\mathrm{N}}{\mathrm{mm}^2} & \text{if } \boldsymbol{d} = \boldsymbol{n}_S \end{cases} \tag{41}$$

Here, the normals

$$\boldsymbol{n}_1 = \frac{(\boldsymbol{g}_1 + \boldsymbol{g}_2)}{\sqrt{2}}, \tag{42a}$$

$$\boldsymbol{n}_2 = \frac{(\boldsymbol{g}_1 + \boldsymbol{g}_3)}{\sqrt{2}}, \tag{42b}$$

$$\boldsymbol{n}_3 = \frac{(\boldsymbol{g}_2 + \boldsymbol{g}_3)}{\sqrt{2}}, \text{ and} \tag{42c}$$

$$\boldsymbol{n}_S = \frac{(\boldsymbol{g}_1 + \boldsymbol{g}_2 + \boldsymbol{g}_3)}{\sqrt{3}} \tag{42d}$$

have been introduced. Thereby, $\boldsymbol{n}_i \; \forall \, i = \{1, 2, 3\}$ are face diagonals ($\langle 110 \rangle$, $\langle 101 \rangle$, and $\langle 011 \rangle$) while $\boldsymbol{n}_S$ is a space diagonal ($\langle 111 \rangle$) of the cubic primitive cell. Again, $\boldsymbol{g}_i \; \forall \, i = \{1, 2, 3\}$ are directions of the crystals orthonormal basis ($\langle 100 \rangle$, $\langle 010 \rangle$, and $\langle 001 \rangle$). Angle brackets used here refer to Miller indizes (Miller, 1839). The orientation dependent Young's modulus can be plotted according to the procedure discussed in Nordmann et al. (2018)[1], which is based on the work of Rychlewski (1995) and Böhlke and Brüggemann (2001). In doing so, we derive the graphical representation given at the left-hand side of Fig. 1. This plot visualizes the directional dependence of Young's modulus for a single crystal. It becomes obvious for cubic silicon, that

$$Y(\boldsymbol{n}_S) = Y_{\max} \qquad \text{and} \qquad Y(\boldsymbol{g}_i) = Y_{\min} \tag{43}$$

hold true. Both values are elementary bounds of the single crystal elasticity. Material parameters determined according to the procedure given in Sect. 2 are given in Tab. 1. There, additionally, the bandwidths spanned

- by the single crystal minimum and maximum values $\Delta_Y^{\min\max} = Y_{\max} - Y_{\min}$,
- by the Voigt and Reuss bounds $\Delta_Y^{\mathrm{VR}} = Y^{\mathrm{V}} - Y^{\mathrm{R}}$, and
- by the arithmetic and geometric means thereof $\Delta_Y^{\mathrm{H\pm}} = Y^{\mathrm{H+}} - Y^{\mathrm{H-}}$

are given. The bandwidths of resulting Poisson's ratios given there are determined in analogous manner. Considering the Young's moduli determined, the right-hand side of Fig. 1 visualizes the directional dependence of all estimates for the polycrystalline aggregate. Clearly, since these estimates are isotropic approximations, the Young's modulus body is spherical.

4 Comparison and Discussion

All further evaluations refer to Young's modulus as it is the substantial parameter, at least in isotropic material engineering. On the other hand, Poisson's ratio of polycrystalline silicon has not been well studied experimentally and hardly any data is available. Firstly, the bandwidths resulting from the bounding values determined here are shown in Fig. 2. Considering first the single

[1] See also: https://tinyurl.com/visualising-elastic-anisotropy

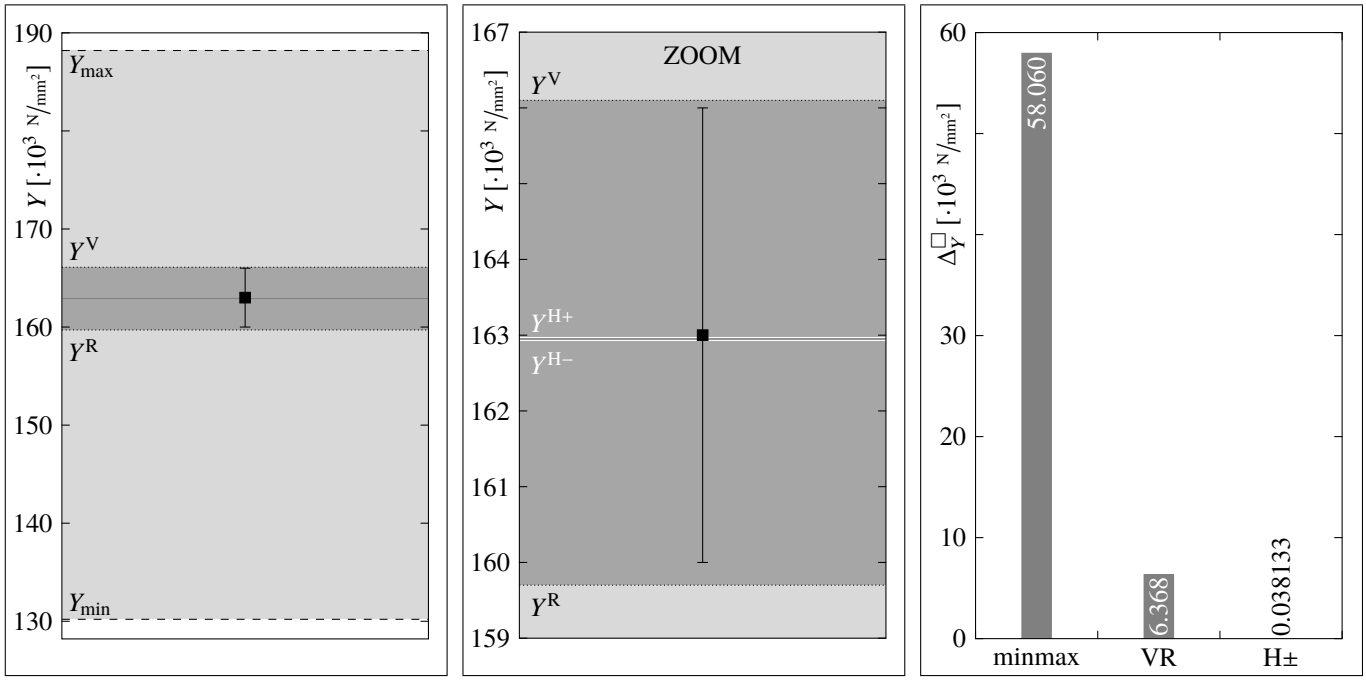

Fig. 2: Spans of extremes and isotropic bounds as well as scattering of experimental results within these ranges (■ - experiments)

crystal extremes we notice a large bandwidth ($\Delta_Y^{\mathrm{minmax}} \approx 58.0 \cdot 10^3\,\mathrm{N/mm^2}$) which doubles the statements for Young's modulus scattering of Petersen (1982). The bandwidth of Voigt and Reuss bound is considerably smaller ($\Delta_Y^{\mathrm{minmax}} \approx 6.4 \cdot 10^3\,\mathrm{N/mm^2}$, about 11% of $\Delta_Y^{\mathrm{minmax}}$). Hill's bounds span a comparatively small band of $\Delta_Y^{\mathrm{H\pm}} \approx 38.1\,\mathrm{N/mm^2}$ which is around 0.6% of the Voigt-Reuss bandwidth. For comparison we use experimental data from Michalicek et al. (1995). Unfortunately, in Michalicek et al. (1995), no tolerance for these measurements is given. Following the compilations of Sharpe (2002), there is a minimal measurement scattering of $\pm 3 \cdot 10^3\,\mathrm{N/mm^2}$ depending on the experimental method for determining the Young's modulus. For visualizational purposes we therefore use $Y^{\mathrm{exp}} = (163.0 \pm 3) \cdot 10^3\,\mathrm{N/mm^2}$ as experimental reference in context of Fig. 2. Obviously, the effective value of YoungâĂŹs modulus is slightly smaller than the mean of the experimental results, at least in the light of $Y^{\mathrm{H+}}$ and $Y^{\mathrm{H-}}$. Thereby we can recognize that the scattering of these experiments lies in between Voigt and Reuss bound. However, these bandwidths are juxtaposed comparatively in Fig. 2 on the right-hand side. We additionally can state the distances of Young's moduli in form of scalar values, indicating an absolute error.

$$d_Y^{\square} = Y^{\square} - Y^{\mathrm{exp}} \qquad \forall\, \square \in \{\mathrm{max}, \mathrm{min}, \mathrm{V}, \mathrm{R}, \mathrm{H+}, \mathrm{H-}\} \tag{44}$$

The results are visualized in Fig. 3, left-hand side. Clearly, the distances to the extremes of the monocrystal are the largest. Distances to Voigt and Reuss bounds are smaller by an order of magnitude. These bounds are almost symmetric around the experimental mean. Hills averages are smaller by two orders of magnitude compared to Voigt-Reuss bounds. Both of Hill's averages are smaller than the experimental mean, i.e. we underestimate the experimental findings by present strategy. Obviously the absolute value of Hill's arithmetic mean $d_Y^{\mathrm{H+}}$ is closest to the experimental mean. Ultimately this underlines the choice of the arithmetic mean according to Hill (1952), at least for present investigations. For further comparison with respect to experimental findings, we analyze the ratio between experimental mean and computed value of Young's modulus.

$$YR^{\square} = \frac{Y^{\square}}{Y^{\mathrm{exp}}} \qquad \forall\, \square \in \{\mathrm{max}, \mathrm{min}, \mathrm{V}, \mathrm{R}, \mathrm{H+}, \mathrm{H-}\} \tag{45}$$

Results of this ratio are visualized in Fig. 3, center. Minimum and Maximum values of the single crystal range around to the experimental value with approximately $^{+0.15}_{-0.20} Y^{\mathrm{exp}}$. Voigt and Reuss bounds significantly reduce this ratios to around $^{+0.02}_{-0.02} Y^{\mathrm{exp}}$. This is being undercut by Hill's averages by two orders of magnitude ($^{-0.0002}_{-0.0004} Y^{\mathrm{exp}}$). Here we can also identify the closest approximation with $Y^{\mathrm{H+}}$ to the experiments. We furthermore introduce the relative error of present estimates.

$$e_Y^{\square} = \frac{d_Y^{\square}}{Y^{\mathrm{exp}}} \qquad \forall\, \square \in \{\mathrm{V}, \mathrm{R}, \mathrm{H+}, \mathrm{H-}\} \tag{46}$$

These measures are given in Fig. 3, right-hand side. It turns out that the error caused when working with Voigt and Reuss estimates is below ±2%. This error is decreased to approximately −0.04% when working with Hill's geometric mean and finally to around −0.02% when applying Hill's arithmetic mean.

In spite of all the numerical deviations determined here, we have to consider the scattering of the experimental results of around $\pm 3 \cdot 10^3\,\mathrm{N/mm^2}$. In this context we have to register $\Delta_Y^{\mathrm{S\pm}} \approx 6 \cdot 10^3\,\mathrm{N/mm^2}$, $d_Y^{\mathrm{S+}} \approx 3 \cdot 10^3\,\mathrm{N/mm^2}$, $d_Y^{\mathrm{S-}} \approx -3 \cdot 10^3\,\mathrm{N/mm^2}$, $YR^{\mathrm{S+}} \approx 1.0184$, $YR^{\mathrm{S-}} \approx 0.9816$, $e_Y^{\mathrm{S+}} \approx 1.8 \cdot 10^{-2}$, and $e_Y^{\mathrm{S-}} \approx -1.8 \cdot 10^{-2}$ while the superscript index S± indicates the bounds resulting from scattering. The error caused by the scattering in the experimental findings causes an error of around 1.8%. As already visualized in Fig. 2 (center), this clarifies that the experimental findings vary in the range of the Voigt-Reuss bounds.

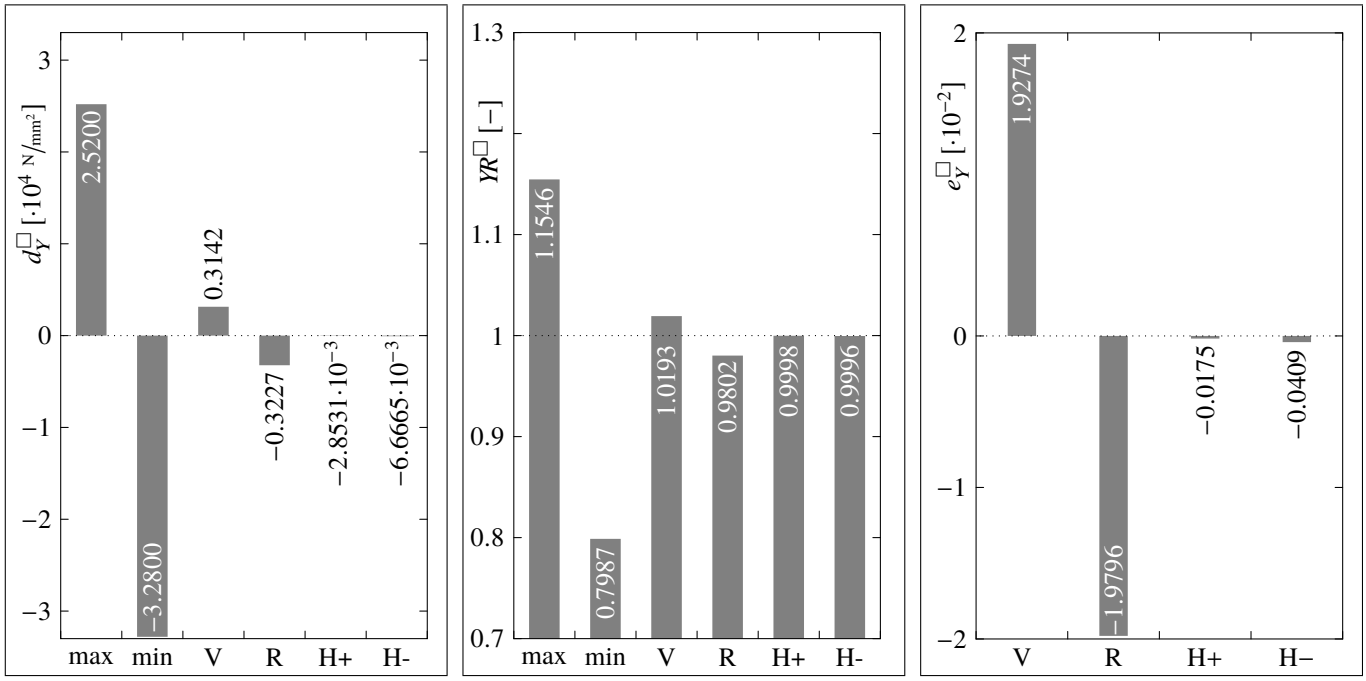

Fig. 3: Distances and ratios of experimental to calculated solutions and associated relative error of Young's modulus estimations

5 Summary and Conclusions

In the foregoing investigations we have predicted the elastic properties of polycrystalline silicon used for solar cells. The predictions were determined by the aid of first-order estimates of analytical homogenization methods. These estimates are based on assumptions for macroscopic homgeneity and isotropy for aggregates of cubic crystals. The whole procedure is based on simplest bounds followed by empirical averages. Present homogenization approach is being applied by the aid of the eigenprojector representation. The advantage of this approach is that we can reduce the tensorial quantities to scalar ones, i.e. this simplifies the computation considerably. This is also an advantage in comparison to computations often done via laborious matrix computations, cf. den Toonder et al. (1999). Based on the invariance of the first eigenvalue of the stiffness (or bulk modulus), the calculus is reduced to the second and third eigenvalue, i.e. the computations reduce to Eqs. (28) and (32).

In context of the results gained therewith when applied to silicon we may conclude that it is sufficient to use Voigt and Reuss bounds and determine the arithmetic mean value proposed by Hill. The latter one predicts the experimental value with sufficient accuracy, i.e. for the given effective material properties, $\mathbb{C}^{\mathrm{H+}}$ is a reasonable approximation for $\bar{\mathbb{C}}$. The quality of this prediction can basically be improved by increasing the order of approximation. This means that the bandwidths of the upper and lower bounds are becoming smaller and smaller. The application of such improvements remains contestable, at least in context of the scattering of the Young's moduli determined at polycrystalline silicon. For polycrystalline silicon, the results imply that the procedure well known as Voigt-Reuss-Hill average provides sufficiently accurate results.

However, the use of silicon for mechanical structures is widespread, so the parameters for this material have been investigated thoroughly. Therefore, the initial values of present calculations, cf. Eq. (39), may scatter to a certain extent ($\pm 500\,\mathrm{N/mm^2}$). In the present treatise we waived the representation of the error propagation caused by the scattering of initial material parameters of the monocrystal. This surely is a problem of experimental mechanics which also concerns the measurements on polycrystalline silicon for solar cells. To counter this problem, sensitive measurements are required at both, the constituents forming the aggregate and the aggregate itself, while one always has to consider the accuracy of the measurement equipment. This is also dependent on the method used, e.g. tension, bending, resonance, indentation, ultrasonic, or bulge test respectively.

The morphology and topology of the material can have an important influence on the effective properties which cannot be considered by the isotropic Voigt and Reuss estimates. For more precise computations, one will have to consider the crystallographic texture, cf. Morawiec (2004). Hereby, the extent of anisotropic effects strongly depends on the degree of crystallographic texture. However, in this case one must consider that both, Voigt and Reuss bounds are anisotropic, i.e. $\|\mathbb{C}^{\mathrm{aniso}}\| = \|\mathbb{C}^{\square} - \mathbb{C}^{\circ}\| \neq 0 \;\forall \square \in \{\mathrm{V}, \mathrm{R}\}$. On the one hand this needs theoretical considerations for the analysis of textures, which can be found in the literature Kocks et al. (1998). On the other hand, experimental investigations on crystal orientation distribution functions of polycrystalline silicon aggregates used for solar cells are necessary to feed such models. Such studies however, are absent.

Acknowledgement

This work was triggered during a visit stay at Griffith University (Australia) while the first author was fellow of the German Research Foundation (grant number 83477795), whose support he very gratefully acknowledges. He furthermore likes to thank Andreas Öchsner for his kind hospitality during this stay. The topic was stimulated by discussions with Zia Javanbakht, to whom he wishes to express many thanks.

Appendix

A.1 Equivalent vector-matrix based procedure

In engineering, especially in the geometrically linear setting of classical continuum theory, a vector-matrix representation finds broad application. This is possible since present mechanical problem is set in the space of symmetric tensors. To be exact, the stress $\boldsymbol{T} = T_{ij}\boldsymbol{e}_i \otimes \boldsymbol{e}_j$ and strain tensor $\boldsymbol{E} = E_{kl}\boldsymbol{e}_k \otimes \boldsymbol{e}_l$ are symmetric, i.e.

$$\begin{aligned} \boldsymbol{a}\cdot\boldsymbol{T} &= \boldsymbol{T}\cdot\boldsymbol{a} & \boldsymbol{T} &= \boldsymbol{T}^\top & T_{ij} &= T_{ji} \\ \boldsymbol{a}\cdot\boldsymbol{E} &= \boldsymbol{E}\cdot\boldsymbol{a} & \boldsymbol{E} &= \boldsymbol{E}^\top & E_{kl} &= E_{lk} \end{aligned}$$

and the constitutive tensor $\mathbb{C} = C_{ijkl}\boldsymbol{e}_i \otimes \boldsymbol{e}_j \otimes \boldsymbol{e}_k \otimes \boldsymbol{e}_l$ features left sub-symmetry, right sub-symmetry and major symmetry, i.e.

$$\begin{aligned} \boldsymbol{A}:\mathbb{C}:\boldsymbol{B} &= \boldsymbol{B}:\mathbb{C}:\boldsymbol{A} & C_{ijkl} &= C_{klij} & &\text{major symmetry} \\ \boldsymbol{A}:\mathbb{C} &= \boldsymbol{A}^\top:\mathbb{C} & C_{ijkl} &= C_{jikl} & &\text{left subsymmetry} \\ \mathbb{C}:\boldsymbol{A} &= \mathbb{C}:\boldsymbol{A}^\top & C_{ijkl} &= C_{ijlk} & &\text{right subsymmetry} \end{aligned}$$

for arbitrary $\boldsymbol{a}, \boldsymbol{A}, \boldsymbol{B}$. Due to the symmetries given we can uniquely assign vectors and matrices to these tensors. In accordance with the operations in Sect. 2, we can then execute the algebraic operations analogously in a vector-matrix notation. To derive such a representation we first introduce a six-dimensional basis (Brannon, 2018), which we will call Kelvin basis, cf. Thomson (1856).

$$\boldsymbol{K}_i = \boldsymbol{e}_i \otimes \boldsymbol{e}_i \qquad \forall\, i = \{1,2,3\} \tag{A.1a}$$

$$\boldsymbol{K}_{3ND-i-j} = \frac{\sqrt{2}}{2}\left[\boldsymbol{e}_i \otimes \boldsymbol{e}_j + \boldsymbol{e}_j \otimes \boldsymbol{e}_i\right] \qquad \forall\, i,j = \{1,2,3\} \text{ while } i < j \tag{A.1b}$$

Herein, ND is the number of dimensions under consideration ($ND = 3$). Obviously our ordering is in accordance with classical Voigt notation (Voigt, 1889), while the normalization with $\sqrt{2}$ differs from the classical representation where only the symmetric part is applied. Since the index of these second-order bases is running from 1 to 6, we introduce greek indices so that $\boldsymbol{K}_\alpha\ \forall\, \alpha = \{1,\dots,6\}$ holds. The Kelvin basis is orthonormal.

$$\boldsymbol{K}_\alpha:\boldsymbol{K}_\beta = \delta_{\alpha\beta} \tag{A.2}$$

A six-dimensional vector representation of stresses and strains is possible while the components are defined as follows.

$$T_\alpha = \boldsymbol{T}:\boldsymbol{K}_\alpha \qquad \forall\, \alpha = \{1,\dots,6\} \tag{A.3a}$$

$$E_\beta = \boldsymbol{E}:\boldsymbol{K}_\beta \qquad \forall\, \beta = \{1,\dots,6\} \tag{A.3b}$$

Both vectors are related by a six-by-six-matrix which is based on the constitutive tensor. We can determine the coefficients of this constitutive matrix by the following calculation rule.

$$C_{\alpha\beta} = \boldsymbol{K}_\alpha:\mathbb{C}:\boldsymbol{K}_\beta \qquad \forall\, \alpha,\beta = \{1,\dots,6\} \tag{A.4}$$

Due to the calculation rules shown, all indices of the vector-matrix notation (α, β) can be assigned to the tensor notation (i, j, k, l), and vice versa. Thus, the tensors $\boldsymbol{T}, \boldsymbol{E}, \mathbb{C}$ may also be written as follows.

$$\boldsymbol{T} = T_\alpha\ \boldsymbol{K}_\alpha \tag{A.5a}$$

$$\boldsymbol{E} = E_\beta\ \boldsymbol{K}_\beta \tag{A.5b}$$

$$\mathbb{C} = C_{\alpha\beta}\,\boldsymbol{K}_\alpha \otimes \boldsymbol{K}_\beta \tag{A.5c}$$

We can achieve the vector-matrix representation of the constitutive law by the arrangement of the coefficients.

$$\begin{bmatrix} T_1 \\ T_2 \\ T_3 \\ T_4 \\ T_5 \\ T_6 \end{bmatrix} = \begin{bmatrix} C_{11} & C_{12} & C_{13} & C_{14} & C_{15} & C_{16} \\ & C_{22} & C_{23} & C_{24} & C_{25} & C_{26} \\ & & C_{33} & C_{34} & C_{35} & C_{36} \\ & & & C_{44} & C_{45} & C_{46} \\ & & & & C_{55} & C_{56} \\ \text{sym} & & & & & C_{66} \end{bmatrix} \begin{bmatrix} E_1 \\ E_2 \\ E_3 \\ E_4 \\ E_5 \\ E_6 \end{bmatrix} \tag{A.6}$$

Herein, the matrix $[C_{\alpha\beta}]$ takes the general anisotropic form. For the sake of completeness we provide the assignment of the parameters with indices i, j, k, l and α, β. These are relations of the stresses

$$T_1 = T_{11} \qquad T_2 = T_{22} \qquad T_3 = T_{33} \qquad T_4 = \sqrt{2}T_{23} \qquad T_5 = \sqrt{2}T_{13} \qquad T_6 = \sqrt{2}T_{12},$$

the strains

$$E_1 = E_{11} \qquad E_2 = E_{22} \qquad E_3 = E_{33} \qquad E_4 = \sqrt{2}E_{23} \qquad E_5 = \sqrt{2}E_{13} \qquad E_6 = \sqrt{2}E_{12},$$

and the constitutive coefficients for an aelotropic material

$$\begin{aligned}
&C_{11} = C_{1111} \quad C_{12} = C_{1122} \quad C_{13} = C_{1133} \quad C_{14} = \sqrt{2}C_{1123} \quad C_{15} = \sqrt{2}C_{1113} \quad C_{16} = \sqrt{2}C_{1112}\\
&\qquad\qquad C_{22} = C_{2222} \quad C_{23} = C_{2233} \quad C_{24} = \sqrt{2}C_{2223} \quad C_{25} = \sqrt{2}C_{2213} \quad C_{26} = \sqrt{2}C_{2212}\\
&\qquad\qquad\qquad\qquad C_{33} = C_{3333} \quad C_{34} = \sqrt{2}C_{3323} \quad C_{35} = \sqrt{2}C_{3313} \quad C_{36} = \sqrt{2}C_{3312}\\
&\qquad\qquad\qquad\qquad\qquad\qquad C_{44} = 2C_{2323} \quad C_{45} = 2C_{2313} \quad C_{46} = 2C_{2312}\\
&\qquad\qquad\qquad\qquad\qquad\qquad\qquad\qquad C_{55} = 2C_{1313} \quad C_{56} = 2C_{1312}\\
&\qquad\qquad\qquad\qquad\qquad\qquad\qquad\qquad\qquad\qquad C_{66} = 2C_{1212},
\end{aligned}$$

while $C_{\alpha\beta} = C_{\beta\alpha}$ holds. This modified representation was already used, e.g., by Fedorov (1968). When introducing sans serif, upright, bold minuscules for vectors and sans serif, upright, bold majuscules for matrices, we can write generalized Hooke's law of Eq. (A.6) in the form $\mathbf{t} = \mathbf{C}\,\mathbf{e}$. Due to the normalization factor introduced in Eq. (A.1b), the following relations between vector-matrix and tensor notation hold.

$$\mathbf{t}^{\top}\mathbf{t} = \boldsymbol{T}\!:\!\boldsymbol{T} \qquad \mathbf{e}^{\top}\mathbf{e} = \boldsymbol{E}\!:\!\boldsymbol{E} \qquad \mathbf{t}^{\top}\mathbf{e} = \boldsymbol{T}\!:\!\boldsymbol{E} \tag{A.7}$$

Furthermore, $\mathbf{C}$ features the same invariants, eigenvalues, and eigendirections as $\mathbb{C}$ and obeys the major symmetry (Nordmann et al., 2018). The normalization also enables to apply operations like trace, determinant, matrix multiplications and so on at componentens of six-by-six matrices.[2] In context of cubic symmetry, the occupiedness of $\mathbf{C}$ reduces as follows when lattice basis and (sample) reference basis coincide.

$$\mathbf{C}^{\mathrm{c}} = \begin{bmatrix} C_{11} & C_{12} & C_{12} & 0 & 0 & 0\\ & C_{11} & C_{12} & 0 & 0 & 0\\ & & C_{11} & 0 & 0 & 0\\ & & & C_{44} & 0 & 0\\ & & & & C_{44} & 0\\ \mathrm{sym} & & & & & C_{44} \end{bmatrix} \qquad \text{with} \quad \begin{aligned} C_{11} &= C_{1111}\\ C_{12} &= C_{1122}\\ C_{44} &= 2C_{2323} \end{aligned} \tag{A.8}$$

Obviously we can identify $C_{11} = {}^1\!/_3(\lambda_1^c + 2\lambda_2^c)$, $C_{12} = {}^1\!/_3(\lambda_1^c - \lambda_2^c)$, and $C_{44} = {}^1\!/_2\lambda_3^c$ and find a projector representation for the elasticity matrix in analogy to Eq. (16) (Halmos, 1958). As was introduced at the elasticity matrix in Eq. (A.4), we determine matrix coefficients of the projectors also.

$$(P_{\alpha\beta})_J^{\mathrm{c}} = \boldsymbol{K}_\alpha\!:\!\mathbb{P}_J^{\mathrm{c}}\!:\!\boldsymbol{K}_\beta \qquad \forall\, \alpha = \{1,\dots,6\} \wedge J = \{1,\dots,3\} \tag{A.9}$$

Ordering all coefficients, the cubic projectors are represented by six-by-six matrices as follows.

$$\mathbf{P}_1^{\mathrm{c}} = \begin{bmatrix} \frac{1}{3} & \frac{1}{3} & \frac{1}{3} & 0 & 0 & 0\\ & \frac{1}{3} & \frac{1}{3} & 0 & 0 & 0\\ & & \frac{1}{3} & 0 & 0 & 0\\ & & & 0 & 0 & 0\\ & & & & 0 & 0\\ \mathrm{sym} & & & & & 0 \end{bmatrix} \quad \mathbf{P}_2^{\mathrm{c}} = \begin{bmatrix} \frac{2}{3} & -\frac{1}{3} & -\frac{1}{3} & 0 & 0 & 0\\ & \frac{2}{3} & -\frac{1}{3} & 0 & 0 & 0\\ & & \frac{2}{3} & 0 & 0 & 0\\ & & & 0 & 0 & 0\\ & & & & 0 & 0\\ \mathrm{sym} & & & & & 0 \end{bmatrix} \quad \mathbf{P}_3^{\mathrm{c}} = \begin{bmatrix} 0 & 0 & 0 & 0 & 0 & 0\\ & 0 & 0 & 0 & 0 & 0\\ & & 0 & 0 & 0 & 0\\ & & & 1 & 0 & 0\\ & & & & 1 & 0\\ \mathrm{sym} & & & & & 1 \end{bmatrix} \tag{A.10}$$

This representation holds only when the refence vectors of the orthonormal system are lattice vectors. In this context we can write the constitutve matrix as sum of eigenvalues and corresponding projection matrices.

$$\mathbf{C}^{\mathrm{c}} = \lambda_1^{\mathrm{c}}\mathbf{P}_1^{\mathrm{c}} + \lambda_2^{\mathrm{c}}\mathbf{P}_2^{\mathrm{c}} + \lambda_3^{\mathrm{c}}\mathbf{P}_3^{\mathrm{c}} \tag{A.11}$$

The compliance $\mathbf{S} = \mathbf{C}^{-1}$ is determined through $\mathbf{S}\,\mathbf{C}^{-1} = \mathbf{1}$ while $\mathbf{1}$ is the identity matrix.

$$\mathbf{S}^{\mathrm{c}} = \frac{1}{\lambda_1^{\mathrm{c}}}\mathbf{P}_1^{\mathrm{c}} + \frac{1}{\lambda_2^{\mathrm{c}}}\mathbf{P}_2^{\mathrm{c}} + \frac{1}{\lambda_3^{\mathrm{c}}}\mathbf{P}_3^{\mathrm{c}} \tag{A.12}$$

[2] For instance, the present strategy to reduce to a vector-matrix notation keeps us from an incorrect determination of the eigenvalues of the stiffness matrix as done through various softwares circulating out there. However, when original Voigt notation is used, $\lambda_J(\mathbf{C}) = \lambda_J(\mathbb{C})$ has no general validity since the physical parameters C_{ijkl} in $\mathbf{C}$ are not normalized with the metric.

For the sake of completeness we give the cubic compliance in terms of the coefficients $C_{\alpha\beta}$.

$$\mathbf{S}^{\mathrm{c}} = \begin{bmatrix} S_{11} & S_{12} & S_{12} & 0 & 0 & 0 \\ & S_{11} & S_{12} & 0 & 0 & 0 \\ & & S_{11} & 0 & 0 & 0 \\ & & & S_{44} & 0 & 0 \\ & & & & S_{44} & 0 \\ \mathrm{sym} & & & & & S_{44} \end{bmatrix} \quad \text{with} \quad \begin{aligned} S_{11} &= \frac{C_{11}+C_{12}}{(C_{11}-C_{12})(C_{11}+2C_{12})} \\ S_{12} &= \frac{-C_{12}}{(C_{11}-C_{12})(C_{11}+2C_{12})} \\ S_{44} &= \frac{1}{C_{44}} \end{aligned}$$

Herein, $S_{11} = {(2\lambda_1^c + \lambda_2^c)}/{(3\lambda_1^c\lambda_2^c)}$, $S_{12} = {(\lambda_2^c - \lambda_1^c)}/{(3\lambda_1^c\lambda_2^c)}$, and $S_{44} = {2}/{\lambda_3^c}$ hold. In analogy to the tensorial description we can give representations of Voigt and Reuss homogenization schemes in matrix notation, cf. Eq. (24).

$$\mathbf{C}^{\mathrm{V}} = \sum_{\gamma=1}^{\eta} v_\gamma \mathbf{C}_\gamma^{\mathrm{c}} \qquad \mathbf{S}^{\mathrm{R}} = \sum_{\gamma=1}^{\eta} v_\gamma \mathbf{S}_\gamma^{\mathrm{c}} \qquad \forall\, \eta \in \mathcal{N}^+ \tag{A.14}$$

The isotropic constitutive law can be written as follows.

$$\mathbf{C}^\circ = \lambda_1^\circ \mathbf{P}_1^\circ + \lambda_2^\circ \mathbf{P}_2^\circ \tag{A.15}$$

Applying the isotropic projectors of Eq. (27) in Eq. (A.9) yields the components $(P_{\alpha\beta})_J^\circ \;\forall\, J = \{1,2\}$. The equivalent matrix representation for isotropic projectors is then given as follows.

$$\mathbf{P}_1^\circ = \begin{bmatrix} \frac{1}{3} & \frac{1}{3} & \frac{1}{3} & 0 & 0 & 0 \\ & \frac{1}{3} & \frac{1}{3} & 0 & 0 & 0 \\ & & \frac{1}{3} & 0 & 0 & 0 \\ & & & 0 & 0 & 0 \\ & & & & 0 & 0 \\ \mathrm{sym} & & & & & 0 \end{bmatrix} \qquad \mathbf{P}_2^\circ = \begin{bmatrix} \frac{2}{3} & -\frac{1}{3} & -\frac{1}{3} & 0 & 0 & 0 \\ & \frac{2}{3} & -\frac{1}{3} & 0 & 0 & 0 \\ & & \frac{2}{3} & 0 & 0 & 0 \\ & & & 1 & 0 & 0 \\ & & & & 1 & 0 \\ \mathrm{sym} & & & & & 1 \end{bmatrix} \tag{A.16}$$

Here again $\mathbf{P}_1^\circ = \mathbf{P}_1^c = \mathbf{P}_1$ holds. The isotropic elasticity matrix can be presented as $\left[C_{\alpha\beta}\right]^\circ = \mathbf{C}^\circ$.

$$\mathbf{C}^\circ = \begin{bmatrix} C_{11} & C_{12} & C_{12} & 0 & 0 & 0 \\ & C_{11} & C_{12} & 0 & 0 & 0 \\ & & C_{11} & 0 & 0 & 0 \\ & & & C_{44} & 0 & 0 \\ & & & & C_{44} & 0 \\ \mathrm{sym} & & & & & C_{44} \end{bmatrix} \quad \text{with} \quad \begin{aligned} C_{11} &= \frac{Y^\circ(1-\nu^\circ)}{(1-2\nu^\circ)(1+\nu^\circ)} \\ C_{12} &= \frac{Y^\circ\nu^\circ}{(1-2\nu^\circ)(1+\nu^\circ)} \\ C_{44} &= \frac{Y^\circ}{2(1+\nu^\circ)} \end{aligned} \tag{A.17}$$

Herein, the material parameters Y° and ν° hold for all isotropic approximations $\circ \in \{\mathrm{V}, \mathrm{R}, \mathrm{H}+, \mathrm{H}-\}$. Alternatively we can state the three isotropic coefficients $C_{\alpha\beta}$ in terms of K° and G°,

$$C_{11} = K^\circ + \frac{4}{3}G^\circ \qquad C_{12} = K^\circ - \frac{2}{3}G^\circ \qquad C_{44} = G^\circ, \tag{A.18}$$

or in terms of λ_1° and λ_2°.

$$C_{11} = \frac{1}{3}(\lambda_1^\circ + 2\lambda_2^\circ) \qquad C_{12} = \frac{1}{3}(\lambda_1^\circ - \lambda_2^\circ) \qquad C_{44} = \lambda_2^\circ, \tag{A.19}$$

The homogenization is here also based on the eigenvalues $\lambda_J^c \;\forall\, J \in \{2,3\}$ while applying Eqs. (28) and (32). Again, $\lambda_1^c = \lambda_1^\circ = \lambda_1^\square \;\forall\, \square \in \{\mathrm{V}, \mathrm{R}, \mathrm{H}+, \mathrm{H}-\}$ holds. Finally we can present the results in form of constitutive matrices of the different estimates by the aid of projectors.

$$\mathbf{C}^\square = \lambda_1 \mathbf{P}_1 + \lambda_2^\square \mathbf{P}_2^\circ \qquad \forall\, \square \in \{\mathrm{V}, \mathrm{R}, \mathrm{H}+, \mathrm{H}-\} \tag{A.20}$$

The present procedure naturally yields identical results as given in Tab. 1.

A.2 Equivalence of different respresentations of Hooke's laws

Engineers are usually confused about the projector representation of constitutive laws. We here want to verify the equivalence of different representations of Hooke's law, at least in the case of isotropy. We start with the projector representation of the constitutive tensor

$$\mathbb{C}^\circ = \lambda_1^\circ \mathbb{P}_1^\circ + \lambda_2^\circ \mathbb{P}_2^\circ \tag{A.21}$$

while we want to point out that the isotropic projectors $\mathbb{P}_1^\circ$ and $\mathbb{P}_2^\circ$ map the strain tensor $\boldsymbol{E}$ into its dilatoric and deviatoric part, respectively.

$$\mathbb{P}_1^\circ \colon \boldsymbol{E} = \boldsymbol{E}^{\mathrm{dil}} \qquad \mathbb{P}_2^\circ \colon \boldsymbol{E} = \boldsymbol{E}^{\mathrm{dev}} \tag{A.22}$$

This dil-dev split is additive.

$$\boldsymbol{E} = \boldsymbol{E}^{\mathrm{dil}} + \boldsymbol{E}^{\mathrm{dev}} \tag{A.23}$$

We can thus write our constitutive law $\boldsymbol{T} = \mathbb{C}^\circ \colon \boldsymbol{E}$ as follows.

$$\boldsymbol{T} = \lambda_1^\circ \boldsymbol{E}^{\mathrm{dil}} + \lambda_2^\circ \boldsymbol{E}^{\mathrm{dev}} \tag{A.24}$$

Using the relations of Eq. (36) yields a well-known form of Hooke's law.

$$\boldsymbol{T} = 3K\boldsymbol{E}^{\mathrm{dil}} + 2G\boldsymbol{E}^{\mathrm{dev}} \tag{A.25}$$

In the light of (A.23) we can reformulate this representation.

$$\boldsymbol{T} = 3K\boldsymbol{E}^{\mathrm{dil}} + 2G(\boldsymbol{E} - \boldsymbol{E}^{\mathrm{dil}}) \tag{A.26a}$$

$$= 3K\boldsymbol{E}^{\mathrm{dil}} + 2G\boldsymbol{E} \; - 2G\boldsymbol{E}^{\mathrm{dil}} \tag{A.26b}$$

$$= (3K - 2G)\,\boldsymbol{E}^{\mathrm{dil}} + 2G\boldsymbol{E} \tag{A.26c}$$

We already know that $\boldsymbol{E}^{\mathrm{dil}} = \frac{1}{3}[\boldsymbol{E} \colon \boldsymbol{1}]\boldsymbol{1}$ holds and obtain the following representation.

$$\boldsymbol{T} = \left(K - \frac{2}{3}G\right)[\boldsymbol{E} \colon \boldsymbol{1}]\boldsymbol{1} + 2G\boldsymbol{E} \tag{A.27}$$

We furthermore introduce the first ($\lambda = K - {}^2\!/_3 G$, please note that this λ is without any index) and the second LamÃľ parameter ($\mu = G$), cf. Lamé (1852).

$$\boldsymbol{T} = \lambda[\boldsymbol{E} \colon \boldsymbol{1}]\boldsymbol{1} + 2\mu\boldsymbol{E} \tag{A.28}$$

We are aware that $\boldsymbol{E} \colon \boldsymbol{1} = \mathrm{tr}\boldsymbol{E}$. However, Eq. (A.28) is known as LamÃľ representation, established in civil engineering. As the relations

$$\lambda = \frac{\nu Y}{(1-2\nu)(1+\nu)} \qquad \text{and} \qquad \mu = \frac{1}{2}\frac{Y}{(1+\nu)} \tag{A.29}$$

hold in the case of isotropy , we can also write the constitutive law in the form

$$\boldsymbol{T} = \frac{\nu Y}{(1-2\nu)(1+\nu)}[\boldsymbol{E} \colon \boldsymbol{1}]\boldsymbol{1} + \frac{Y}{(1+\nu)}\boldsymbol{E} \tag{A.30}$$

which seems to be more familiar to mechanical engineers.

References

P. A. Basore. Defining terms for crystalline silicon solar cells. *Progress in Photovoltaics: Research and Applications*, 2(2): 177–179, 1994. doi: 10.1002/pip.4670020213.

T. Böhlke and C. Brüggemann. Graphical representation of the generalized Hooke's law. *Technische Mechanik*, 21(2):145–158, 2001. URL http://www.uni-magdeburg.de/ifme/zeitschrift_tm/2001_Heft2/Boehlke_Brueggeman.pdf.

H. J. Böhm. A Short Introduction to Continuum Micromechanics. ILSB Report 207, Institute of Lightweight Design and Structural Biomechanics (ILSB), Vienna University of Technology, Vienna, Austria, 2020. URL https://www.ilsb.tuwien.ac.at/links/downloads/ilsbrep206.pdf.

R. M. Brannon. *Rotation, Reflection, and Frame Changes: Orthogonal tensors in computational engineering mechanics*. IOP Publishing, Bristol, 2018. doi: 10.1088/978-0-7503-1454-1.

H. J. Bunge. Zur Darstellung allgemeiner Texturen. *Zeitschrift für Metallkunde*, 56(-):872–874, 1965.

R. M. Christensen and K. H. Lo. Solutions for effective shear properties in three phase sphere and cylinder models. *Journal of the Mechanics and Physics of Solids*, 27(4):315–330, 1979. doi: 10.1016/0022-5096(79)90032-2.

J. M. J. den Toonder, J. A. W. van Dommelen, and F. P. T. Baaijens. The relation between single crystal elasticity and the effective elastic behaviour of polycrystalline materials: theory, measurement and computation. *Modelling and Simulation in Materials Science and Engineering*, 7(6):909–928, 1999. doi: 10.1088/0965-0393/7/6/301.

A. A. Elvin. Number of grains required to homogenize elastic properties of polycrystalline ice. *Mechanics of Materials*, 22(1): 51–64, 1996. doi: 10.1016/0167-6636(95)00024-0.

F. I. Fedorov. *Theory of Elastic Waves in Crystals*. Plenum Press, New York, 1968. doi: 10.1007/978-1-4757-1275-9.

P. R. Halmos. *Finite-Dimensional Vector Spaces*. Springer, New York, 1958. doi: 10.1007/978-1-4612-6387-6.

Z. Hashin and S. Shtrikman. On some variational principles in anisotropic and nonhomogeneous elasticity. *Journal of the Mechanics and Physics of Solids*, 10(4):335–342, 1962a. doi: 10.1016/0022-5096(62)90004-2.

Z. Hashin and S. Shtrikman. A variational approach to the theory of the elastic behaviour of polycrystals. *Journal of the Mechanics and Physics of Solids*, 10(4):343–352, 1962b. doi: 10.1016/0022-5096(62)90005-4.

M. Hayes. Connexions between the moduli for anistropic elastic materials. *Journal of Elasticity*, 2(2):135–141, 1972. doi: 10.1007/BF00046063.

R. Hill. The elastic behaviour of a crystalline aggregate. *Proceedings of the Physical Society. Section A*, 65(5):349–354, 1952. doi: 10.1088/0370-1298/65/5/307.

M. A. Hopcraft, W. D. Nix, and T. W. Kenny. What is the young's modulus of silicon? *Journal of Microelectromechanical Systems*, 19(2):229–330, 2010. doi: 10.1109/JMEMS.2009.2039697.

W. F. Hosford. *The Mechanics of Crystals and Textured Polycrystals*. Oxford University Press, 1993.

U. F. Kocks, C. N. Tomé, H. R. Wenk, A. J. Beaudoin, and H. Mecking. *Texture and Anisotropy: Preferred Orientations in Polycrystals and Their Effect on Materials Properties*. Cambridge University Press, 1998.

M. Köntges, S. Kurtz, C. Packard, U. Jahn, K. A. Berger, K. Kato, T. Friesen, H. Liu, and M. Van Iseghem. Review of failures of pv modules, 2014. URL http://iea-pvps.org/fileadmin/dam/intranet/ExCo/IEA-PVPS_T13-01_2014_Review_of_Failures_of_Photovoltaic_Modules_Final.pdf.

E. Kröner. Berechnung der elastischen Konstanten des Vielkristalls aus den Konstanten des Einkristalls. *Zeitschrift für Physik*, 151(4):504–518, 1958. doi: 10.1007/BF01337948.

E. Kröner. *Statistical continuum mechanics*. Number 92 in CISM International Centre for Mechanical Sciences. Springer, 1972. doi: 10.1007/978-3-7091-2862-6.

G. Lamé. *Leçons sur la théorie mathématique de l'élasticité des corps solides*. Bachelier, 1852. URL https://gallica.bnf.fr/ark:/12148/bpt6k5747708p.

M. Lobos Fernãndez. *Homogenization and materials design of mechanical properties of textured materials based on zeroth-, first- and second-order bounds of linear behavior*. PhD thesis, Karlsruher Institut für Technologie (KIT), 2018.

M. M. Mehrabadi and S. C. Cowin. Eigentensors of linear anisotropic elastic materials. *The Quarterly Journal of Mechanics and Applied Mathematics*, 43(1):15–41, 1990. doi: 10.1093/qjmam/43.1.15.

M. A. Michalicek, D. E. Séné, and V. M. Bright. Advanced modeling of micromirror devices. In *Proceedings of the International Conference on Integrated Micro/Nanotechnology for Space Applications*, pages 224–239, Houston, 1995.

W. H. Miller. *A Treatise on Crystallography*. Deighton, Cambridge, 1839. URL https://archive.org/details/treatiseoncrysta00millrich.

A. Morawiec. *Orientations and Rotations: Computations in Crystallographic Textures*. Springer, Berlin Heidelberg, 2004. doi: 10.1007/978-3-662-09156-2.

S. Nemat-Nasser and M. Hori. *Micromechanics: Overall Properties of Heterogeneous Solids*. Elsevier, New York, 1993.

J. Nordmann, M. Aßmus, and H. Altenbach. Visualising elastic anisotropy: Theoretical background and computational implementation. *Continuum Mechanics and Thermodynamics*, 30(4):689–708, 2018. doi: 10.1007/s00161-018-0635-9.

K. E. Petersen. Silicon as a mechanical material. *Proceedings of the IEEE*, 70(5):420–457, 1982. doi: 10.1109/PROC.1982.12331.

S. Philipps and W. Warmuth. Photovoltaics report. Technical report, Fraunhofer Institute for Solar Energy Systems, Freiburg i.Br., Germany, November 2019.

S. I. Ranganathan and M. Ostoja-Starzewski. Universal elastic anisotropy index. *Phys. Rev. Lett.*, 101:055504–1–4, 2008. doi: 10.1103/PhysRevLett.101.055504.

M. Nygårds. Number of grains necessary to homogenize elastic materials with cubic symmetry. *Mechanics of Materials*, 35(11): 1049–1057, 2003. doi: 10.1016/S0167-6636(02)00325-3.

A. Reuss. Berechnung der Fließgrenze von Mischkristallen auf Grund der Plastizitätsbedingung für Einkristalle. *Zeitschrift für Angewandte Mathematik und Mechanik*, 9(1):49–58, 1929. doi: 10.1002/zamm.19290090104.

J. Rychlewski. On Hooke's law. *Journal of Applied Mathematics and Mechanics*, 48(3):303–314, 1984. doi: 10.1016/0021-8928(84)90137-0.

J. Rychlewski. Unconventional approach to linear elasticity. *Archives of Mechanics*, 47(5):149–171, 1995.

J. Rychlewski and J. M. Zhang. Anisotropic Degree of Elastic Materials. *Archives of Mechanics*, 41(5):697–715, 1989.

W. N. Sharpe. chapter Mechanical properties of MEMS materials. CRC Press, Boca Raton, 2002.

G. Stokkan, A. Song, and B. Ryningen. Investigation of the grain boundary character and dislocation density of different types of high performance multicrystalline silicon. *Crystals*, 8(9), 2018. doi: 10.3390/cryst8090341.

S. Sutcliffe. Spectral Decomposition of the Elasticity Tensor. *Journal of Applied Mechanics*, 59(4):762–773, 1992. doi: 10.1115/1.2894040.

W. Thomson. Elements of a mathematical theory of elasticity. *Philosophical Transactions of the Royal Society of London*, 146: 481–498, 1856. URL http://www.jstor.org/stable/108596.

W. Voigt. Über die Beziehung zwischen den beiden Elasticitätskonstanten isotroper Körper. *Wiedemann´sche Annalen*, 38: 573–587, 1889. doi: 10.1002/andp.18892741206.

L. J. Walpole. Fourth-rank tensors of the thirty-two crystal classes: Multiplication tables. *Proceedings of the Royal Society of London. Series A, Mathematical and Physical Sciences*, 391(1800):149–179, 1984. URL http://www.jstor.org/stable/2397534.

Y. M. Yang, A. Yu, B. Hsu, W. C. Hsu, A. Yang, and C. W. Lan. Development of high-performance multicrystalline silicon for photovoltaic industry. *Progress in Photovoltaics: Research and Applications*, 23(3):340–351, 2015. doi: 10.1002/pip.2437.

C. M. Zener. *Elasticity and Anelasticity of Metals*. University of Chicago press, Chicago, 1948.